2026 European Conference on Computing in Construction
Corfu, Greece
July 12-15, 2026

A TWO-STAGE MEP INSTALLATION CONSTRUCTABILITY OPTIMIZATION SYSTEM INTEGRATING DSM-BASED MODULE DIVISION AND 4D SIMULATION

Ang Li[1], Zhengyi Chen[2], and Jack C.P. Cheng[1]
[1] The Hong Kong University of Science and Technology, Hong Kong SAR, China
[2] Southeast University, Nanjing, China

Abstract

While modularization techniques can reduce installation complexity and improve the efficiency of MEP projects, existing approaches predominantly focus on static constraints and overlook the dynamic environmental interactions in assembly process. Addressing these challenges, this paper developed an MEP installation optimization framework integrating DSM-based module division and a simulation-based feedback mechanism. The framework extracts IFC data for dynamic modeling, clusters elements into modules, and employs a feedback loop to optimize installation sequences. Validated on a real-world project, the system successfully generates collision-free kinematic paths and significantly reduces installation costs, demonstrating enhanced efficiency and constructability for MEP systems.

Introduction

Mechanical, Electrical, and Plumbing (MEP) systems are essential in building systems, providing essential services to maintain a comfortable environment (Wang et al., 2025). However, the installation of these systems is challenging due to their inherent complexity, characterized by high component density and intricate spatial layouts (Lee, 2014). Consequently, the installation constructability of MEP systems, defined as the ease and efficiency of installation, has become a critical determinant of overall project constructability (Wang et al., 2016). The successful installation of MEP systems within pre-existing building structures relies heavily on a robust installation plan (Wu et al., 2022), specifically the precise sequencing and path planning of components. Suboptimal installation sequences often lead to on-site congestion and spatial conflicts (Yan et al., 2024), severely compromising construction efficiency. Therefore, developing an automated system to optimize the installation plan is imperative for enhancing MEP constructability.

To mitigate the inefficiencies and installation difficulty in traditional on-site MEP installation, off-site modular construction and multi-trade integrated MEP (MiMEP) has been widely adopted in MEP project. This approach divides the MEP system into different modules, then pre-fabricates and pre-installs the module to reduce the on-site installation (Zhao et al., 2026), thereby enhancing the installation constructability. For MiMEP, the installation plan includes determining the module division and determining the installation sequence and path for each module. However, the granularity of module division (i.e., module dimension and quantity) critically dictates the feasibility of the delivery path (Zhao et al., 2024). Determining the optimal module division remains a significant challenge, as it must balance the benefits of prefabrication against the rigorous spatiotemporal constraints imposed by the constructed environment.

Existing matrix-based methodologies have demonstrated significant efficacy in MEP modularization. For example, Samarasinghe et al. (2019) utilized the Dependency Structure Matrix (DSM) to quantify the interaction strength between MEP components, which effectively clusters MEP elements into cohesive modules. However, current module division methods predominantly prioritize static physical constraints, such as stiffness, structural integrity, and weight. Consequently, these methods often fail to adequately account for the dynamic environmental interactions inherent to the installation process, specifically overlooking critical factors like transportation trajectories and evolving spatial availability.

Furthermore, current research usually formulates the MEP installation sequences schedule as a mathematical optimization problem to determine optimal sequence. For instance, Yin et al. (2024) modeled the sequencing task using mixed integer linear programming (MILP), aiming to minimize potential spatial conflicts. However, such approaches often overlook the reciprocal influence between the installation sequence and the dynamic site environment, which fails to consider how an installed module alters the feasible path planning for subsequent components. Moreover, these methods typically lack a quantitative framework for evaluating installation costs and efficiency. Therefore, integrating 4D simulation into the optimization framework is necessary, as it provides a dynamic testbed that can rigorously capture the evolving spatiotemporal environment, ensuring that the continuous changes in site constraints are fully accounted for during sequence planning.

For the implementation of 4D simulation, the Robot Operating System (ROS) has emerged as a predominant platform. It offers a robust ecosystem featuring advanced physics engines and modular libraries that enable high-fidelity modeling of kinematic interactions and collision dynamics (Kim et al., 2021). While recent studies have successfully demonstrated the conversion of building information modeling (BIM) data into ROS environments for general construction simulations (Liang et al., 2025), research specifically targeting the complex domain of MEP systems remains limited. Furthermore, given that MEP optimization inherently involves evolving spatiotemporal constraints, there is a distinct lack of a unified framework that effectively integrates 4D simulation with the dynamic constraint management required for the MEP installation process.

Addressing this contextual backdrop, this paper proposes a two-stage MEP installation optimization framework that integrates DSM-based module division and 4D simulation. The system aims to generate optimal installation sequences and collision-free kinematic paths, thereby maximizing constructability within the dynamic on-site environment.

Methodology

To enhance installation constructability through precise sequence planning, this study proposes a comprehensive MEP installation optimization framework driven by 4D simulation, presented in Figure 1. The methodology comprises three integral steps: 1) Dynamic environmental modeling, this step extracts constructability-related data from IFC files to instantiate a physics-based 4D simulation environment within the ROS; 2) MEP module division, a DSM-based approach is employed to decompose complex MEP systems into discrete, manageable modules, thereby facilitating off-site prefabrication and on-site assembly. 3) Installation sequence optimization, the optimal installation sequence and kinematic paths are determined via a two-stage optimization algorithm with feedback mechanisms.

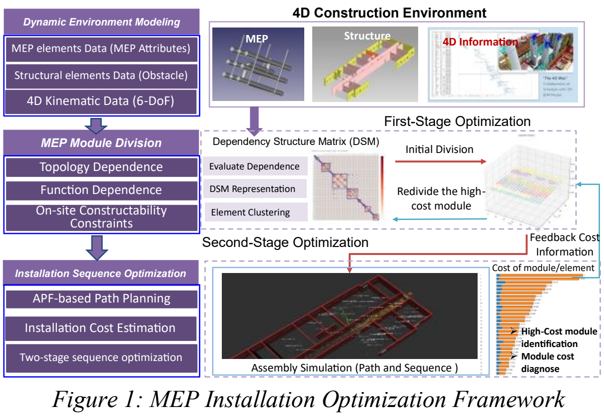

Figure 1: MEP Installation Optimization Framework

Dynamic environment modeling for MEP installation

To address the complexities of the dynamic construction environment, this study establishes a high-fidelity kinematic model (Robot Operating System, ROS) of the dynamic environment, which can precisely simulate the installation trajectories of MEP components to calculate installation cost and analyze sequence conflicts, thereby supporting subsequent optimization of installation paths and sequences. The establishment of dynamic environment involves two steps: (1) Extraction of Constructability-related Information from IFC data, and (2) Establishment of kinematic simulation environment within ROS.

Extraction of Constructability-related information from IFC data

To facilitate the precise extraction of constructability-related data for MEP installation, the IfcOpenShell library is employed to parse the BIM data in Industry Foundation Classes (IFC) files. Table 1 summarizes the specific instances of the MEP and structural elements extracted to support the optimization process. The study focuses on four fundamental categories of MEP elements: segments, fittings, controllers, and terminals. These categories encompass the primary components of MEP systems and provide a sufficient basis for analyzing and enhancing installation constructability. Additionally, structural elements, specifically entities under IfcBuildingElement, are extracted and treated as static obstacles (i.e., spatial constraints) during the installation process.

Table 1: Constructability-related IFC Information

Element	Entity	MEP Instance
MEP Element	IfcFlowSegment	IfcPipeSegment IfcDuctSegment IfcCableSegment
	IfcFlowFitting	IfcPipeFitting IfcDuctFitting IfcCableFitting
	IfcFlowController	IfcValve IfcFlowMeter IfcSwitchingDevice
	IfcFlowTerminal	IfcAirTerminal
Structural Elements	IfcBuildingElement	IfcWall IfcColum IfcBeam IfcSlab

To support dynamic modeling, the constructability-related information for each MEP element (the target of the optimization) is categorized into three distinct domains:

1) Geometric Information: The geometric configuration and spatial positioning of MEP elements are prerequisites for developing the assembly kinematics model used in installation simulations. The shape representation of each element is derived from IfcShapeRepresentation and stored as a triangulated boundary representation (B-Rep). Furthermore, the position of each element is retrieved from IfcObjectPlacement and transformed into a unified global coordinate system by traversing the relevant chain of local coordinate systems.

2) Production Information: This domain encompasses critical fabrication and installation attributes, including material type (e.g., galvanized steel, PVC), assembly method (e.g., flange, weld), and element weight. These attributes significantly influence the complexity of MEP

installation. For instance, modules requiring heterogeneous assembly methods necessitate frequent switching between different tooling or processes on-site, thereby increasing installation difficulty. Regarding data extraction, material types are queried from the IfcMaterial of the associated entities, while assembly methods are derived from specific property sets (e.g., Pset_DistributionPortTypeDuct) attached to IfcDistributionPort. Additionally, element weights are retrieved directly from IfcQuantityWeight.

3) Functional Information: This category defines the functional classification of an MEP element and its functional-related elements. The functional classification of the element identifies the specific purpose of an element (e.g., pipe system or duct system) and is used for clustering elements based on their utility. This information is extracted from the PredefinedType attribute (e.g., IfcDuctSegmentTypeEnum) of the respective IFC entities. Furthermore, the functional-related elements refer to the connected elements to ensure the systemic functionality, which can be derived from IfcRelConnectsElements or IfcRelFlowControlElements of the associated entities.

Establishment of Simulation Environment for Path and Sequence Planning

To develop the simulation test platform, the extracted IFC information is instantiated within the ROS environment (Figure 2), which defines the boundary specifications (obstacles) and environmental constraints necessary for MEP elements installation. The ROS environment provides a physics-based computational framework that enables spatiotemporal optimization of construction sequences and installation path planning under dynamic on-site environmental constraints.

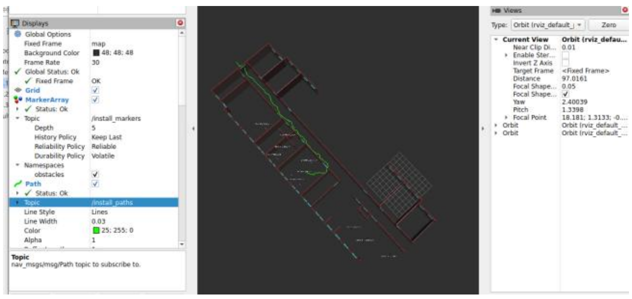

Figure 2: Interface of ROS

The configuration of ROS for 4D installation optimization includes 3 parts as follows:

1) Static Environmental Constraints: Structural elements (e.g., columns, beams, and slabs) completed prior to the MEP phase are instantiated as static rigid bodies. These elements serve as hard constraints, explicitly delineating the occupied volumetric space that must be avoided during the operation.

2) Traversable Space Definition: The system identifies architectural openings, such as corridors, doors, and windows, to define the navigable volume. This volume maps the available free space designated for the logistical transport of MEP components.

3) Configuration Space Configuration: By integrating the static structural data with the traversable volume, the environment establishes a collision-free configuration space. This representation serves as the foundational input for subsequent path planning algorithms, ensuring that any generated trajectory strictly adheres to the physical realities of the partially built structure.

MEP Model Division considering constructability constraints

To mitigate the inefficiencies inherent in traditional on-site MEP installation, off-site modular construction has been widely adopted. This approach decomposes complex, large-scale MEP networks into discrete, manageable modules. These modules are pre-assembled in a controlled off-site environment, thereby reducing on-site operations to relatively simple inter-modular connections. However, determining the optimal division (i.e., quantity and dimensions) of these modules presents a significant challenge, particularly given the spatial constraints imposed by the on-site constraints. The module division strategy critically impacts both assembly cost and installation complexity; therefore, the system must be divided to minimize complex on-site assembly operations.

To obtain the optimum module division, this study develops a dependence structure matrix (DSM)-based framework for module division and facility the module installation. The DSM-based method uses a matrix represent the dependence (i.e., interaction strength) of each MEP elements and cluster the high-dependent elements into a cohesive module. The framework comprises two primary stages: (1) Evaluation of MEP element dependence in DSM; (2) Module division considering on-site constraints.

Evaluation of MEP element dependence in DSM

The interdependence of the MEP elements is depicted in matrix form using DSM, which identifies the clusters of the elements have stronger inner interactions by mapping the interaction between elements in the system. DSM typically has a square symmetric matrix, where the diagonal axis of the matrix represents the elements and off-diagonal points represent the dependent value of one element with another.

The dependence values are estimated based on Eq. (1), which includes two components i.e., the topology dependence and function dependence. The detailed indexes for dependence estimation is shown in Table 2.

$$d = d_{Topology} + d_{Function} \quad (1)$$

Module division considering on-site constraints

The module division phase employs a Constrained Agglomerative Clustering algorithm to group MEP elements into different modules. This process is governed by a greedy optimization strategy as the following stages:

1) Prioritization via Greedy Strategy: To maximize intra-module cohesion, the algorithm prioritizes element pairs with the strongest coupling. All elements (D_{ij}) in the DSM are sorted in descending order based on their dependent value. This ensures that elements with the highest

Table 2: MEP elements dependence evaluation

Dependence type	Index	Description
Topology Dependence	Connectivity Constraint	If two elements are physically connected (i.e., sharing a common flow port or joint), the dependency $d_{Topology}$ score is incremented by 1.
	Adjacent Elements	To account for potential spatial clustering, the $d_{Topology}$ score is incremented by 1 if the Euclidean distance between two elements is less than a predefined threshold of 0.5 meters.
	Loop Integrity	If elements constitute a closed-loop sub-system or a local hydraulic cycle (e.g., bypass piping loops, valve manifolds), their $d_{Topology}$ score is incremented by 1 to preserve the integrity of these functional groups during modularization.
Function Dependence	Homogeneity	The $d_{Function}$ score is increased by 1 if the pair of elements belongs to the same IFC entity class or functional category, ensuring consistency in component handling.
	Process Compatibility	The $d_{Function}$ score is incremented by 1 if the elements share identical connection mechanisms or assembly interfaces (e.g., flange-to-flange connections)
	Operational Coupling	The $d_{Function}$ score is incremented by 1 for element pairs exhibiting operational interdependency

topological and functional dependencies are evaluated for merging with higher priority.

2) Cluster Aggregation Process: Initially, each MEP element is treated as a discrete singleton cluster. The algorithm iterates through the sorted dependence value. For any two distinct clusters with high dependence value, a tentative merge operation is initiated to form a potential candidate module.

3) Dynamic Constraint Verification: Before finalizing the union of two clusters, the candidate module must pass a rigorous feasibility check to ensure compliance with on-site limitations (e.g., logistics and installation), which is shown in Table 3. The Union operation is executed if and only if the candidate module satisfies all constraints. If a constraint violation is detected, the merge is rejected, and the clusters remain independent to prevent the formation of infeasible super-modules.

Table3: The on-site constraints for module division

Constraint	Description
Dimensional Constraints	The geometric dimensions of each module are validated against the maximum transportable envelope (e.g., $3m \times 6m \times 4m$) determined by project logistics.
Payload Constraints	The cumulative mass of the module must strictly adhere to the rated lifting capacity of the on-site hoisting equipment.
Gravity Stability	The module's center of gravity is constrained to fall strictly within its support footprint to guarantee static stability during hoisting and placement.
Clustering Coefficien	A module should not contain two dense clusters connected solely by a slender or fragile element, which is extremely prone to breakage during transportation.

Installation Sequence Optimization with feedback mechanism

While off-site modularization significantly mitigates on-site complexity, overall construction efficiency and cost remains critically sensitive to the assembly sequence. A suboptimal sequence often leads to spatial conflicts, where previously installed components obstruct the feasible installation trajectories of subsequent modules. To address this, this study implements a two-stage optimization strategy, it utilizes the Artificial Potential Field (APF) method for path planning, integrated with a feedback mechanism that triggers module redivision when viable paths cannot be found.

<u>Formulation of installation optimization</u>

The objective of the optimization is to obtain installation sequence $S = [m_1, m_2, \dots, m_N]$ with lowest total installation cost, where m_i is the module installed in the i-th step. The objective function can be formulated as Eq. (2). The E_{i-1} is the installation environment for i-th step which includes the static structural elements (e.g., walls, columns) and the installed MEP elements in previous i-1 steps. The installation path should satisfy the collision free constraint as Eq. (3) represented, specifically, for each module m_i , a continuous path must exist that remains strictly collision-free with respect to both static environmental obstacles and the cumulative volume of all previously installed modules $(m_1, \dots, m_{i-1})$.

$$Obj\text{: Min } Cost = \sum_{i=1}^{N} Cost(m_i|E_{i-1}) \quad (2)$$

$$Constraint\text{: Path}_{\mathrm{m}_1} \cap E_{i-1} = \emptyset \quad (3)$$

To calculate the comprehensive installation cost and improve the installation efficiency, the installation cost for m_i consist of the weighted cost of translation and rotation manipulation ($Cost_M$), the cost penalty for operational difficulty caused by proximity ($Cost_P$), the cost for trajectory smoothness ($Cost_S$), which are shown in Eq. (4).

$$Cost_{m_i} = Cost_M + Cost_P + Cost_S \quad (4)$$

$Cost_M$ is calculated based on the length of the installation path, since rotational manipulation typically incurs significantly higher costs and control efforts compared to translational displacement, a higher weight coefficient is assigned to the rotational cost, which is shown in Eq. (5).

$$\mathrm{Cost}_M = \mathrm{w}_1 T + \mathrm{w}_2 RL \quad (5)$$

Where w_1 and w_2 are the weight for translational cost and rotational cost, respectively, $\mathrm{w}_1 < \mathrm{w}_2$, T is the total amount of translational manipulation, R is the total amount of rotational manipulation (rad), L is the length of the module.

The $Cost_P$ quantifies the operational difficulty imposed by spatially constrained environments (e.g., narrow pipe shafts). Limited space increased the control precision of manipulation and reduced the maneuvering speeds.

$$Cost_P = \int_{p_0}^{p_1} \max\big(0, D_S - \mathrm{D}(p,\mathrm{O})\big)\, dp \quad (6)$$

Where p_0 and p_1 are the start point and end point of the path, respectively, D_S is the safe distance between MEP and obstacles, $\mathrm{D}(p,\mathrm{O})$ is the actual distance between MEP and obstacles.

The $Cost_S$ evaluates the geometric continuity of the trajectory. Even in obstacle-free zones, trajectories exhibiting high tortuosity (e.g., frequent sharp turns or erratic zigzag maneuvers) are operationally inefficient due to the requirement for frequent acceleration and deceleration.

$$Cost_S = \sum_{q=1}^{P} \left|\Delta\theta_q\right| L \quad (7)$$

where $\Delta\theta_q$ represents the turning angle (i.e., the change in heading) between adjacent path segments at waypoint q.

The simulation-based heuristic search algorithm employed to determine the optimal installation sequence in ROS platform. Specifically, the proposed approach adopts a Greedy Strategy with Look-ahead to iteratively select the next module for installation. The procedure for each installation step is detailed below:

1) Candidate Generation: To reduce the search space, a subset of potential candidates is identified from the remaining uninstalled module set, denoted as R. A heuristic filter selects the top-K modules ($CandidateSet \subset R$) based on geometric volume, prioritizing larger modules to resolve major spatial constraints early in the sequence.

2) Feasibility Simulation: For each candidate module $c \in CandidateSet$, a physics-based simulation is executed to verify installation feasibility. The system invokes the path planner (using the Artificial Potential Field method in this study) to generate a collision-free trajectory from the supply point to the installation target, considering the current environmental state (static structures plus previously installed modules). Candidates for which a valid path cannot be generated are deemed infeasible in the current iteration.

3) Cost Evaluation and Selection: The installation cost, $Cost(c)$, is computed for each feasible candidate using the multi-objective metric defined previously (incorporating manipulation effort, safety clearance, and path smoothness). The module yielding the minimum cost is selected as the optimal choicem_i for the current step.

4) Dynamic State Update: Upon selection, the geometry of module m_i is instantiated into the simulation environment and registered as a dynamic obstacle. Consequently, the path planning for all subsequent steps $(i+1)$ must strictly avoid the volume occupied by m_i, ensuring the physical validity of the evolving assembly sequence.

<u>Artificial potential field-based module installation path planning</u>

In this study, the APF algorithm is employed as the core trajectory generator, which provides computationally efficient, real-time motion planning with simple mathematical formulation (Liu et al., 2020). The fundamental objective is to compute a collision-free path for each module from its supply point to the installation target. The supply point refers to the storage location of prefabricated MEP components on the construction site. The installation target is the geometric location of the installing MEP element exported from design model.

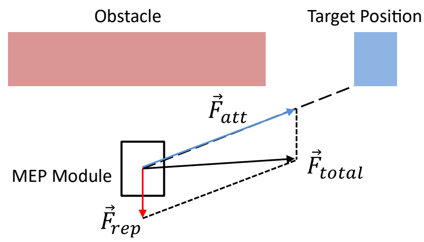

Figure 3: Artificial Potential Field Method

The algorithm conceptually abstracts the MEP module as a point mass moving within a composite virtual force field, driven by the interaction of two distinct potential functions:

1) Attractive Force ($\vec{F}_{att}$) Generated by the target installation position, this force exerts a gravitational-like pull on the module, guiding it towards the destination. The magnitude of the attractive force is typically proportional to the Euclidean distance between the module and the target, ensuring global convergence.

$$\vec{F}_{att} = k_{att} \cdot \left(\vec{P}_{goal} - \vec{P}_{current}\right) \quad (7)$$

Where k_{att} is the coefficient for attractive force.

2) Repulsive Force ($\vec{F}_{rep}$) Generated by obstacles to enforce collision avoidance. The obstacle set comprises static constraints (e.g., structural walls, columns) and dynamic constraints (i.e., the set of previously installed modules). Analogous to magnetic repulsion, these obstacles exert a pushing force that increases exponentially as the module approaches the obstacle boundary (ρ_0), thereby preventing physical intersection.

$$\vec{F}_{rep} = \eta \left(\frac{1}{\rho} - \frac{1}{\rho_0}\right) \frac{1}{\rho^2} \tag{7}$$

Where η is the repulsive gain coefficient.

The motion of the module is governed by the superposition of the attractive and repulsive forces. At each iterative step, the system calculates the resultant force vector acting on the module. The module's position is updated incrementally along the direction of this resultant force (following the negative gradient of the potential field) until it successfully converges at the target coordinates.

$$\vec{F}_{total} = \vec{F}_{att} + \vec{F}_{rep} \tag{7}$$

<u>Feedback high-cost information for module redivision</u>

Suboptimal module partitioning often leads to computational instability during path optimization, manifesting as deadlocks (local minima) or oscillatory trajectories. This typically necessitates excessive manual tuning of stochastic perturbation parameters to achieve convergence. To address this, a closed-loop feedback mechanism is introduced. When a module exhibits an anomalous trajectory, the aggregate navigation cost is decomposed to evaluate the contribution of individual constituent elements within the DSM. An element is identified as a high-cost contributor if it violates specific kinematic or spatial criteria:

Spatial Constriction: The element maintains persistent proximity to obstacles, indicating a clearance bottleneck.

Kinematic Amplification: The element is located at the distal end of the rotation radius, resulting in high linear velocity and an excessive swept volume.

Based on this diagnosis, these high-cost elements are imposed as separation constraints within the DSM to trigger module re-partitioning, followed by a re-optimization of the installation sequence.

Results

Case Description

To rigorously validate the feasibility and robustness of the proposed MEP installation optimization framework, a real-world construction project in Figure 4 was selected as the empirical testbed. This case study represents a large-scale, high-density engineering scenario, comprising 17283 distinct MEP elements and 762 structural entities (e.g., beams, columns, and shear walls). Characterized by its intricate spatial layout and complex topological entanglements, this project presents a significant computational challenge, making it an ideal benchmark to verify the effectiveness of the proposed method in handling high-dimensional combinatorial optimization problems, which need to consider both the module division and installation path.

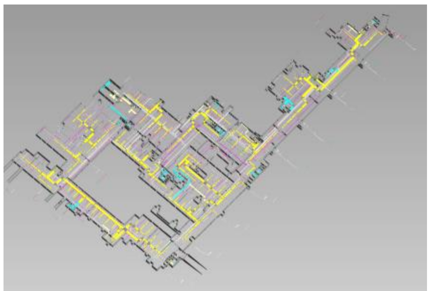

Figure 4: MGY underground parking garage MEP model

Module Division Results

By applying the proposed DSM-based framework which integrates topological dependencies with physical constraints, the 17283 MEP elements in the MEP design were successfully divided into 2564 distinct modules.

To provide a granular visualization of the partitioning efficacy, a representative sub-region comprising 100 contiguous elements was selected for detailed analysis. As illustrated in Figure 5, these elements were algorithmically grouped into 17 modules, where distinct colors denote separate modular assignments. The visualization confirms that physically connected and spatially adjacent components are coherently grouped, ensuring geometric continuity.

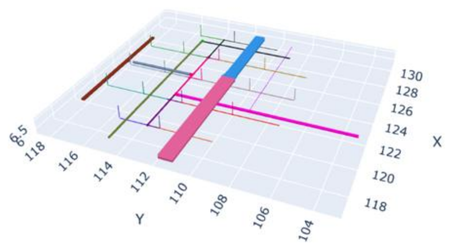

Figure 5: Module division example (100 elements)

The corresponding clustered Dependency Structure Matrix (DSM) is presented in Figure 6. The blue bounding boxes along the main diagonal delineate the boundaries of the identified modules. The heatmap reveals a distinct block-diagonal structure: high-dependency interactions (indicated by darker red hues) are concentrated within the modules, signifying strong intra-module cohesion. Conversely, the sparse distributions outside the diagonal blocks indicate minimal inter-module coupling, validating the algorithm's effectiveness in minimizing complex on-site connections.

Optimization Results

Following the initial module partitioning, the proposed two-stage optimization algorithm was employed to determine the globally optimal installation sequence. Figure 7 illustrates the generated optimal trajectory for a representative module. Crucially, the simulation environment is dynamic; modules scheduled earlier in the sequence are instantiated as static obstacles, thereby enforcing strict spatiotemporal constraints on the current path planning task.

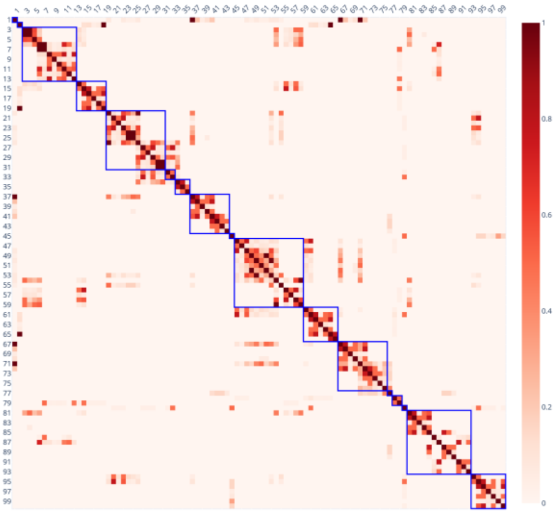

Figure 6: DSM heatmap and element dependence (100 elements)

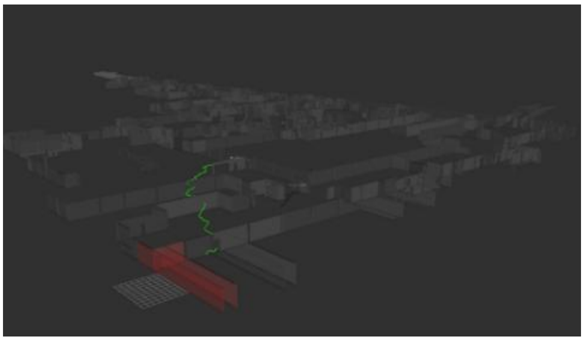

Figure 7: Module installation path diagram

Figure 8 presents the optimized installation sequence and corresponding installation costs for the initial 20 MEP modules. To ensure the installation robustness, the kinematic anomalies of the paths are identified through oscillatory motions detection (i.e., repetitive back-and-forth movements), which is highlighted in red in Figure 8.

These identified anomalies necessitate further optimization via the feedback loop. As illustrated in Figure 9, such kinematic instabilities (e.g., zig-zag trajectories) are often attributed to suboptimal module division, specifically inappropriate module dimensions. The feedback mechanism is utilized to identify high-risk elements that contribute disproportionately to the installation cost.

As detailed in Table 5, these high-risk elements are characterized by high-risk scores (e.g., 0.97), resulting from either persistent proximity to obstacles (high Prox value) or excessive swept volumes due to large rotation radius (Radius close to 1.0). These metrics serve as the basis for imposing separation constraints in the DSM for re-partitioning.

Install Order	Module ID	Module Name	Total Cost
1	MOD_2966	Module MOD_2966	95.99
2	MOD_1283	Module MOD_1283	65.40
3	MOD_2637	Module MOD_2637	156.40
4	MOD_3460	Module MOD_3460	167.79
5	MOD_2649	Module MOD_2649	142.23
6	MOD_527	Module MOD_527	204.97
7	MOD_2627	Module MOD_2627	151.92
8	MOD_2643	Module MOD_2643	219.23
9	MOD_5526	Module MOD_5526	197.75
10	MOD_642	Module MOD_642	243.78
11	MOD_10827	Module MOD_10827	226.76
12	MOD_5830	Module MOD_5830	242.43
13	MOD_1458	Module MOD_1458	274.44
14	MOD_4354	Module MOD_4354	258.99
15	MOD_1276	Module MOD_1276	428.86
16	MOD_4659	Module MOD_4659	247.51
17	MOD_9048	Module MOD_9048	329.98
18	MOD_10447	Module MOD_10447	664.98
19	MOD_10437	Module MOD_10437	726.70
20	MOD_10355	Module MOD_10355	973.94

Figure 8: Module installation sequence

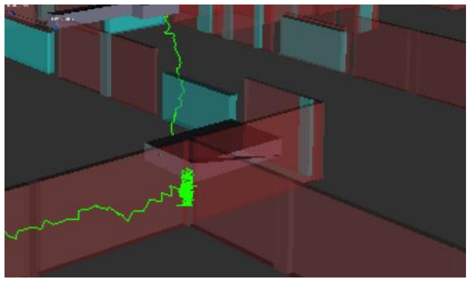

Figure 9: Kinematic anomalies of installation path (Oscillation example)

Table 5: High-Risk Elements (Top 5)

Risk	Swept	Prox	Type	ID
0.97	0.94	1	IfcDuctFitting	8254523
0.74	0.96	0.53	IfcDuctSegment	8254517
0.71	1.00	0.42	IfcDuctFitting	8254538
0.69	0.96	0.42	IfcDuctSegment	8254535
0.66	0.52	0.80	IfcDuctSegment	8254506

Finally, the overall efficacy of the framework is validated through comparative cost analysis.

Table 6: Total installation cost of different method

Method	Optimal Installation cost
Two-stage Optimize	602006
No redivision feedback	1014465
No module division	2752630

As summarized in the comparison Table 6, the proposed two-stage optimization achieves a significant installation cost reduction compared with the baseline methods, which delivers a 78 % lower installation cost than the traditional direct component installation strategy (i.e., without module division) indicating the advantage of modular installation. The two-stage method also shows a 41% cost reduce over no redivision feedback method, confirming that the integration of modularization with feedback-driven optimization yields the most efficient construction process.

Conclusions

To address the critical challenge of modeling dynamic on-site environments and optimizing installation sequences under complex on-site installation constraints, this paper proposes a two-stage MEP installation optimization framework that integrates DSM-based module division and 4D simulation. The system aims to generate optimal installation sequences and collision-free kinematic paths, thereby maximizing constructability within the dynamic on-site environment. Our proposed MEP installation optimization system has three major contributions: 1) IFC-based 4D Simulation Environment, this study establishes 4D simulation environment within ROS, rigorously transforming IFC building information into dynamic spatiotemporal constraints to support virtual construction planning. 2) DSM-based MEP Module Division, the DSM-based framework is developed to streamline off-site fabrication, which employs constrained agglomerative clustering to decompose complex MEP systems into transportable modules based on functional and topological dependence considering on-site constraints. 3) MEP Installation Sequence Optimization with Feedback Mechanism, installation efficiency is maximized via a two-stage sequence optimization algorithm incorporating a closed-loop feedback mechanism, which refines inappropriate module division to resolve kinematic conflicts and path planning deadlocks.

The proposed methodology was validated on a real-world MEP project characterized by high component density and complex layouts. The results indicate that our proposed framework can successfully divide the MEP elements in different modules based on DSM and optimize the installation path and sequence of the MEP module based on 4D simulation. As Table 6 shows, this two-stage MEP installation optimization can significantly reduce the total installation cost, thereby enhancing the installation constructability and efficiency.

With our proposed MEP installation optimization system, users can obtain the robust and collision-free installation plan for MEP project in an efficient and automated way. Additionally, our system leverages the 4D simulation to simulate the changing on-site environment, which can integrate the dynamic installation constraints into the optimization framework. Future research will focus on extending the framework's applicability to more domain-specific and highly complex scenarios, such as intricate HVAC plant room assemblies.

Acknowledgments

The authors would like to thank the Innovation and Technology Fund, HKSAR (No. ITS/394/23FP) for partially supporting this research. The authors declare no known competing financial interests or personal relationships that could have appeared to influence the work reported in this paper.

References

Kim, S., Peavy, M., Huang, P. C., & Kim, K. (2021). Development of BIM-integrated construction robot task planning and simulation system. Automation in Construction, 127, 103720.

Lee, G. (2014). Parallel vs. sequential cascading MEP coordination strategies: A pharmaceutical building case study. Automation in Construction, 43, 170-179

Liang, Z., Yang, L., Liang, Z., Chan, J. C. F., Zhang, Z., Wang, M., & Cheng, J. C. (2025). Optimized UAV view planning for high-quality 3D reconstruction of buildings using a modified sparrow search algorithm. Advanced Engineering Informatics, 65, 103344.

Liu, J., Xu, C., Wu, Z., & Chen, Y. F. (2020). Intelligent rebar layout in RC building frames using artificial potential field. Automation in Construction, 114, 103172.

Samarasinghe, T., Gunawardena, T., Mendis, P., Sofi, M., & Aye, L. (2019). Dependency Structure Matrix and Hierarchical Clustering based algorithm for optimum module identification in MEP systems. Automation in Construction, 104, 153-178.

Wang, B., Lin, F., Li, M., Liang, Z., Chen, Z., Wang, M., & Cheng, J. C. (2025). Informative As-Built Modeling as a Foundation for Digital Twins Based on Fine-Grained Object Recognition and Object-Aware Scan-vs-BIM for MEP Scenes. Advanced Engineering Informatics, 65, 103382.

Wang, J., Wang, X., Shou, W., Chong, H. Y., & Guo, J. (2016). Building information modeling-based integration of MEP layout designs and constructability. Automation in construction, 61, 134-146.

Wu, Q., Chen, L., Shi, P., Wang, W., & Xu, S. (2022). Identifying impact factors of MEP installation productivity: An empirical study. Buildings, 12(5), 565.

Yan, G., Yang, Y., Zhang, H., Li, Z., Chen, S., Zhao, X., ... & Liu, L. (2024). A review of life cycle construction process and cutting-edge technology in prefabricated MEP installation engineering. Buildings, 14(3), 630.

Yin, J., Luo, S., Rui, J., Yao, J., Zhang, F., Fu, B., & Kassem, M. (2024). BIM-based detection and optimization of spatial-temporal clashes in underground pipeline construction. Automation in Construction, 166, 105616.

Zhao, X., Li, J., Yang, Q., Fan, X., Liu, S., Cao, L., ... & Zhang, Z. (2026). Corridor MEP pipeline integration and hanger-layout optimization using BIM-based genetic partitioning and performance analysis. Journal of Intelligent Construction, 9180114.

Zhao, X., Yang, Q., Yan, G., Fan, X., Yang, Y., Zhang, H., & Chen, S. (2024). Length optimization of MEP pipeline integrated modular based on genetic algorithm. Buildings, 14(12), 3826.